Journal of Fluids and Structures (2002) **16**(8), 1093–1110
doi:10.1006/jfls.2002.0465 available online at http://www.idealibrary.com on IDEAL®

EFFECTS OF STEADY ANGLE OF ATTACK ON NONLINEAR GUST RESPONSE OF A DELTA WING MODEL

D. M. Tang, J. K. Henry and E. H. Dowell†

Department of Mechanical Engineering and Materials Science, Duke University Durham North Carolina 27708-0300, U.S.A.

(Received 25 May 2001; and in final form 11 December 2001)

The effects of a steady angle of attack on the nonlinear aeroelastic response of a delta wing model to a periodic gust have been studied. For the theoretical analysis, a three-dimensional time-domain vortex lattice aerodynamic model and a reduced order aerodynamic technique were used and the structure was modelled using von Karman plate theory that allows for geometric strain–displacement nonlinearities in the delta wing structure. Also, an experimental investigation has been carried out in the Duke wind tunnel using a rotating slotted cylinder gust generator and an Ometron VPI 4000 Scanning Laser Vibrometer measurement system to measure deflections (velocities) of a delta wing test model. The fair to good quantitative agreement between theory and experiment verifies that the present analytical approach has reasonable accuracy and good computational efficiency for nonlinear gust response analysis in the time-domain. The results also contribute to a better physical understanding of the nonlinear aeroelastic response of a delta wing model to gust loads when the steady angle of attack is varied.

1. INTRODUCTION

One observation from flight tests is that, by changing the angle of attack of an aircraft, the flight velocity at which limit cycle oscillations (LCOs) begin may be raised or lowered and the amplitude of the LCO may be reduced or increased; see Bunton & Denegri (2000). It has been suggested that this sensitivity to angle of attack indicates the nonlinearity is in the fluid rather than in the structure. Tang & Dowell (2001) have shown theoretically, however, that such effects of an angle of attack change can also be the result of a structural nonlinearity. Tang *et al.* (1999, 2000) presented theoretical and experimental studies of the flutter and limit cycle oscillations, and also the nonlinear aeroelastic response to a periodic gust with zero steady angle of attack of a delta wing. It was shown that the effects of geometric structural nonlinearity for a low aspect ratio plate on the dynamic aeroelastic behavior are not only significant when LCOs occur, but also may be important for response to gust excitation.

Following Tang & Dowell (2001) and Tang *et al.* (1999, 2000), we study here the effects of steady angle of attack on nonlinear aeroelastic response to a periodic gust. A three-dimensional time-domain vortex lattice aerodynamic model and a reduced order aerodynamic technique are used and the structure is modelled using von Karman plate

†Also, Director of the Center for Nonlinear and Complex Systems.

0889-9746/02/081093+18 $35.00/0

theory that allows for geometric strain–displacement nonlinearities in the delta wing structure. To estimate the effects of the steady angle of attack on the response characteristics of a low aspect ratio delta wing plate, a numerical investigation has been made. In order to assess the theoretically predicted gust response characteristics of the delta wing, an experimental investigation has been carried out in the Duke wind tunnel using a RSC gust generator [see Tang *et al.* (1996)], and an Ometron VPI 4000 Scanning Laser Vibrometer measurement system [see Ometron (1997)], to measure deflections (velocities) of the delta wing. The results may be helpful in better understanding physically the nonlinear aeroelastic response of a delta wing model to gust loads when varying the steady angle of attack.

One of the reviewers has observed that, for the maximum effective angle of attack achieved in the experimental study, the possibility exists that leading edge vortices may form, of sufficient intensity that they might be important in modifying the aerodynamic forces on the delta wing. The authors agree that this possibility exists and is worthy of further study. Moreover, certainly there are interesting applications for even larger angles of attack than are considered in the present paper, where leading edge vortices might be important.

2. STATE-SPACE THEORETICAL MODEL

A schematic of the delta wing-plate geometry with a three-dimensional vortex lattice model of the unsteady flow is shown in Figure 1. The aeroelastic structure/fluid state-space model is as follows.

The nonlinear structural model was derived from Lagrange's equations based upon the von Karman plate theory using the total kinetic and elastic energies and the work done by the applied aerodynamic loads on the plate. Modal expansions for the plate deflection are substituted into the energy expressions and then into Lagrange's equations to yield equations of motion for each structural modal coordinate.

For the aerodynamic model, we use a three-dimensional time-domain vortex lattice aerodynamic method and a reduced order aerodynamic technique. In this paper, we

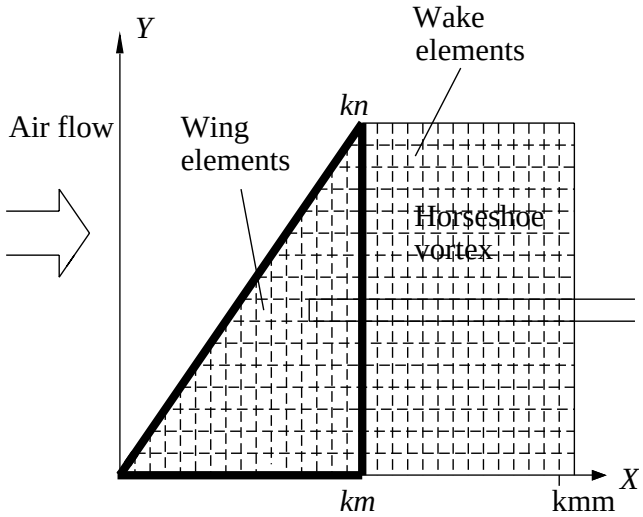

Figure 1. Numerical grid for delta wing-plate using a vortex lattice aerodynamic model; there is a corresponding finite element grid for the structural model (not shown).

assume that the periodic lateral gust is constant along the wing span, i.e., the gust velocity is only a function of chordwise position and time, $w_g = w_g(x, t)$, and it is normalized by airspeed, U. The gust wavelength is defined as

$$l_g = U/\omega,$$

where ω is the gust excitation frequency, in Hz.

A continuous sinusoidal gust time history at the x_i position on the delta wing can be expressed as follows:

$$w_g(x, t) = w_{g0} \sin(2\pi\omega t - \Delta\phi), \tag{1a}$$

where a phase difference is defined as $\Delta\phi = 2\pi x_i/l_g$. Alternatively, an equivalent gust angle of attack is defined as

$$\alpha_g \equiv w_g/U. \tag{1b}$$

A continuous frequency sweep gust is also considered. It is expressed as

$$w_g(x, t) = w_{g0} \sin\left(2\pi\left(\omega_1 + \frac{\omega_2 - \omega_1}{2T}t\right)t - \Delta\phi\right), \tag{2}$$

where ω_1, ω_2 and T are the minimum frequency, maximum frequency, and the sweep duration, respectively.

The flow about the cantilevered plate is assumed to be incompressible, inviscid and irrotational. Here we use an unsteady vortex lattice method to model this flow. A typical planar vortex lattice mesh for the three-dimensional flow is shown in Figure 1. The delta wing and wake are divided into a number of elements. In the wake and on the wing all the elements are of equal size, Δx, in the streamwise direction. Point vortices are placed on the plate and in the wake at the quarter chord of the elements. At the three-quarter chord of each plate element a collocation point is placed for the downwash, i.e., we require the velocity induced by the discrete vortices to equal the total downwash arising from the unsteady motion of the delta wing and also the gust. Thus, an aerodynamic matrix equation can be formed

$$[A]\{\Gamma\}^{t+1} + [B]\{\Gamma\}^{t} = [T]\{w\}^{t+1}, \tag{3}$$

where $[A]$ and $[B]$ are aerodynamic coefficient matrices, $[T]$ is a transfer matrix for determining the relationship between the global vortex lattice mesh and local vortex lattice mesh on the delta wing plate, and $\{w\}^{t+1}$ is the nondimensional downwash at the time step $t + 1$ arising from the unsteady motion, gust loads and the steady angle of attack of the delta wing; it is expressed in matrix form as

$$\{w(x, y)\}^{t+1} = \frac{h}{U}[W(x, y)]\{\dot{q}\}^{t+1} + \frac{h}{c}\left[\frac{\partial W(x, y)}{\partial x}\right]\{q\}^{t+1} + \{\alpha_0(x, y)\} + \frac{1}{U}\{w_g\}^{t+1}, \tag{4}$$

where q is the generalized coordinate of the plate modal deflection in the z-direction and $W(x, y)$ is the transverse modal function in the z-direction. α_0 is a steady angle of attack. Again, w_g is the gust velocity normal to the wing planform.

Thus, combining the nonlinear structural equations and linear aerodynamic equations, we obtain a complete aeroelastic state-space equation based upon a reduced order aerodynamic model using a static correction technique. The final result is given by

(Tang & Dowell 2001; Tang *et al.* 1999, 2000)

$$\begin{bmatrix} I & -Y_{R_a}^{\mathrm{T}}[I - A(A+B)^{-1}]TE \\ C_2 X_{R_a} & D_2 + C_2(A+B)^{-1}TE \end{bmatrix} \begin{Bmatrix} \gamma_d \\ \theta \end{Bmatrix}^{t+1}$$

$$+ \begin{bmatrix} -Z_{R_a} & Y_{R_a}^{\mathrm{T}} B(A+B)^{-1}TE \\ C_1 X_{R_a} & D_1 + C_1(A+B)^{-1}TE \end{bmatrix} \begin{Bmatrix} \gamma_d \\ \theta \end{Bmatrix}^{t}$$

$$= \begin{Bmatrix} 0 \\ -(C_1 + C_2)(A+B)^{-1}T\alpha_0 - F_N/\tau^2 \end{Bmatrix}^{t+1/2}$$

$$+ \begin{bmatrix} Y_{R_a}^{\mathrm{T}}[I - A(A+B)^{-1}] \\ -C_2(A+B)^{-1} \end{bmatrix} \{w_g\}^{t+1} + \begin{bmatrix} -Y_{R_a}^{\mathrm{T}} B(A+B)^{-1} \\ -C_1(A+B)^{-1} \end{bmatrix} \{w_g\}^{t}, \tag{5}$$

where the vector θ is the state of the plate, $\{\theta\} = \{\dot{q}, q\}^{\mathrm{T}}$ and D_1, D_2 are matrices describing the plate structural stiffness and damping behavior. The measured first modal damping ratio, ξ_1, of the delta wing is 0·023. This was used in the gust response calculation. For the higher-order modal damping, we assume that $\xi_n \omega_n = \xi_1 \omega_1$. C_1, C_2 are aerodynamic matrices describing the vortex element distribution on the delta wing. X_{R_a}, Y_{R_a} are the right and left reduced aerodynamic modal eigenvector matrices, and Z_{R_a} is a reduced diagonal matrix whose diagonal entries contain the aerodynamic eigenvalues; γ_d is a reduced vector of the aerodynamic modal coordinates.

3. NUMERICAL RESULTS

The physical model is a simple delta wing configuration with a leading edge sweep of 45°. The model was constructed from $\frac{3}{32}$ in-thick[1] plastic (Lucite material) plate. The root chord was locally clamped (cantilevered), and the length of the cantilever root was 9 in (60-percent root chord). The clamping was symmetric about the center of the root chord of the model. The length of the root chord was 15 in. The aerodynamic vortex lattice model had 120 vortex elements on the delta wing ($km = kn = 15$) and 525 vortex elements in the wake ($kmm = 50$) and nine reduced aerodynamic eigenmodes $R_a = 9$. The numbers of delta wing structural modes were $nxy = 10$ for the out-of-plane and $mxy = 10$ for the in-plane directions, respectively. The mesh of the finite element model for the out-of-plane structural model is 30×30 and thus the delta wing was modelled using 900 quadrilateral plate elements. The mesh of the three-dimensional finite element model for the in-plane structural model is $30 \times 30 \times 1$ and the delta wing was modelled using 961 solid elements with 1921 nodes for the in-plane motion. The nodes at the clamped root chord satisfy fixed geometric boundary conditions, i.e, $w = u = v = \theta_x = \theta_y = \theta_z = 0$. From the finite element model, the out-of-plane and in-plane modes were determined that were used in Lagrange's equations.

3.1. Nonlinear Flutter and LCO for no Gust

The flutter stability of the linearized aeroelastic model of equation (5) is calculated using a dynamic perturbation analysis. The results are shown in Figure 2. The two most important flutter/LCO boundaries versus the steady angle of attack, α_0, are shown in Figure 2(a).

[1] 1 in. = 25·4 mm.

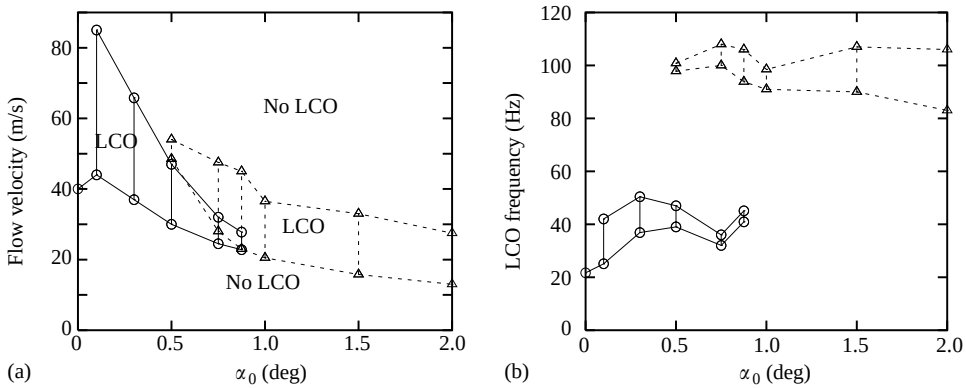

Figure 2. Linearized flutter characteristics versus a steady angle of attack: (a) flutter boundary (flow velocity); (b) flutter frequency. –○–, Lower-mode/lower-frequency flutter boundary; - -Δ- -, higher-mode/higher-frequency flutter boundary.

Figure 2(b) shows the corresponding flutter frequency, ω_f, versus α_0. Note that the flutter behavior has a transition of flutter mode from lower to higher modal participation near $\alpha_0 = 1^\circ$. The flutter velocity is sensitive to the steady angle of attack in the range of $\alpha_0 = 0^\circ \rightarrow 2^\circ$. For more details of the dynamic perturbation analysis, see Tang & Dowell (2001). The lower mode flutter boundary has its primary structural modal participation from natural modes 1–3, while for the higher mode flutter the principal natural modal contributors are 4–6.

3.2. Nonlinear Response to a Single Harmonic Gust Excitation

The theoretical lateral gust angle of attack amplitude, α_{g0}, is initially chosen to be $0{\cdot}75^\circ$, for a single harmonic gust load. We use a time-marching approach to determine the gust response from equation (5). Figure 3 shows the theoretical nondimensional response amplitude, $w_{\text{r.m.s.}}/h$, at the tip calculated for the flow velocities of (a) $U = 10$ m/s, (b) $U = 20$ m/s and (c) $U = 30$ m/s. Note that the transverse deflection, $w_{\text{r.m.s.}}$, is the root-mean-square value of the dynamic or fluctuating response measured relative to the mean time-averaged response. In these figures, the steady angle of attack is $\alpha_0 = 1$ and 2°. For comparison, the results for $\alpha_0 = 0$ are also shown in the Figure 3. As shown in Figure 3(a), the static deflection ($\omega = 0$) increases as the steady angle of attack increases. The peak amplitude of the r.m.s. response occurs at the following gust excitation frequencies: $\omega = 10{\cdot}5$ Hz for $\alpha_0 = 0$, $\omega = 12$ Hz for $\alpha_0 = 1^\circ$ and $\omega = 14$ Hz for $\alpha_0 = 2^\circ$. This increase in the peak frequency is because the static plate transverse deflection increases, and hence the plate stiffness increases as the steady angle of attack increases for a given flow velocity. As found in Tang & Dowell (2001), the dominant structural natural frequency changes with the change in static deflection under the action of the steady aerodynamic loading. From Figure 3(a), we can identify the first "natural frequency" of the aeroelastic model. Of course, this "natural frequency" varies with α_0 and also with U as shown in Figures 3(b) and 3(c). Also, note that there is amplitude jump near the "natural frequency" for $\alpha_0 = 0$ and $u = 10, 20$ and 30 m/s, but it is less pronounced for $\alpha_0 = 1$ and 2°.

Typical time histories and corresponding FFT analysis for different gust excitation frequencies, $\omega_g = 0, 4$ and 10 Hz are shown in Figure 4(a,b) for $\alpha_0 = 1^\circ$ and $U = 30$ m/s. As shown in Figure 2, LCO occur from $U = 20{\cdot}5$ to $36{\cdot}5$ m/s. In this case, there are limit cycle oscillations with a higher frequency and smaller amplitude for no gust load, $\omega_g = 0$.

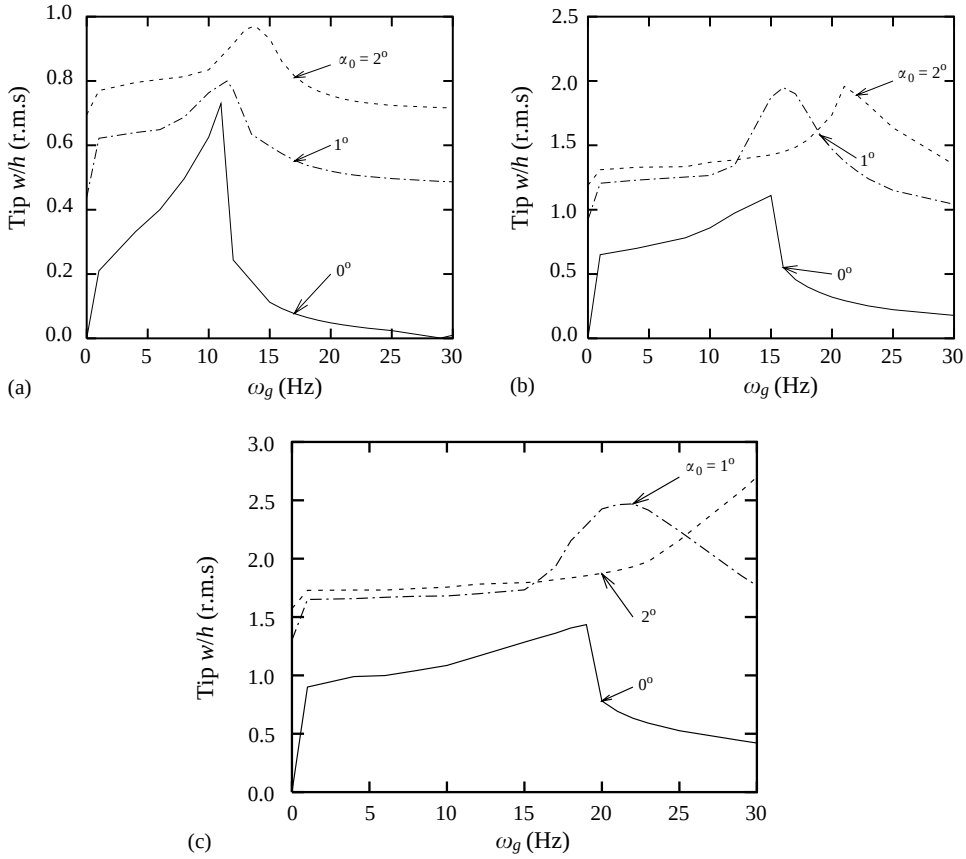

Figure 3. Nonlinear r.m.s. tip deflection response (normalized by the wing thickness) versus gust excitation frequency: (a) $U = 10$ m/s, (b) $U = 20$ m/s, (c) $U = 30$ m/s.

With a gust load and $\omega_g = 4$ and 10 Hz, the response amplitudes are much larger than the LCO amplitude and the higher harmonic components are relatively small. The responses are dominated by the gust loads.

Figure 5 shows nondimensional transverse deflection versus flow velocity for $\alpha_0 = 0$, 1 and 2°. Figures 5(a) and 5(b) correspond to the gust excitation frequencies, 10 and 20 Hz, respectively. As shown in Figure 5(a) for $\omega_g = 10$ Hz, the r.m.s. amplitude increases as the flow velocity and the steady angle of attack increase. The total deflection is dominated by the static deflection, i.e., the dynamic response is small compared to the static deflection. The dynamic deflection *per se* is less important, because the gust excitation frequency is lower than the "natural frequency" of this aeroelastic model. However for $\alpha_0 = 1°$, we did find a small dynamic peak response near $U = 25$ m/s as shown in Figure 6(a) for the velocity response at the wing tip. In this figure, we only show the r.m.s. dynamic response measured with respect to the static deflection shape taken as the reference. The r.m.s. dynamic response decreases as the steady angle of attack increases for a given flow velocity. When the gust excitation frequency is 20 Hz, there is a resonant response near $U = 30$ m/s for $\alpha_0 = 1°$ and $U = 17{\cdot}5$ m/s for $\alpha_0 = 2°$, as shown in Figures 5(b) and 6(b). These results can be understood as arising from the nonlinear stiffening of the wing structure as it deforms statically and dynamically.

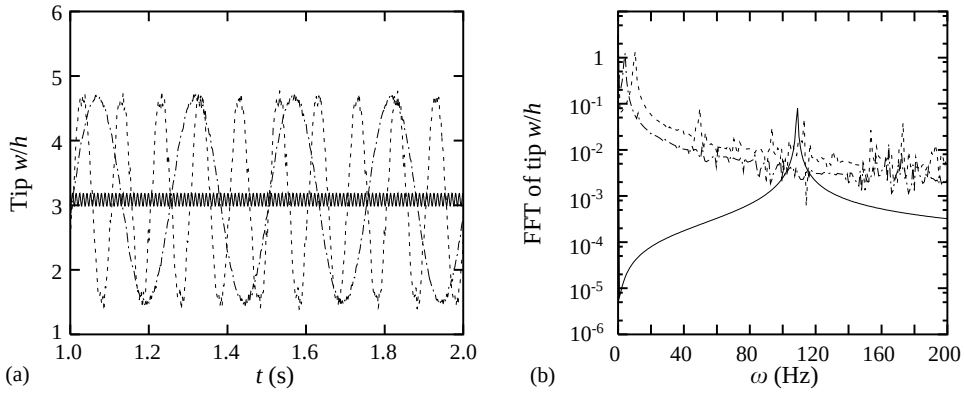

Figure 4. Nonlinear deflection response to a single harmonic gust for $U = 30$ m/s and $\alpha_0 = 1^\circ$: (a) time history; (b) FFT analysis. LCO with : —, no gust; —●–, $w_g = 4$ Hz; - - - -, $w_g = 10$ Hz.

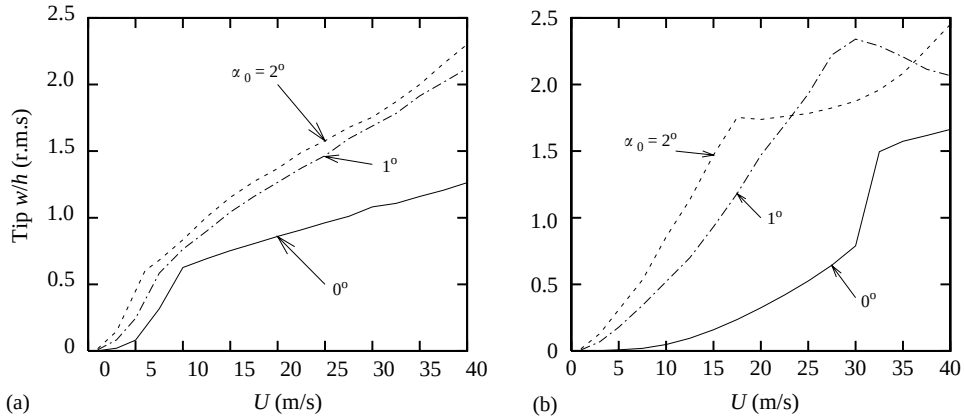

Figure 5. Nondimensional r.m.s. transverse deflection versus flow velocity: (a) $\omega_g = 10$ Hz; (b) $\omega_g = 20$ Hz.

3.3. Nonlinear Response to a Frequency Sweep Gust Excitation

For the theoretical model of the linear frequency sweep gust excitation, the gust angle of attack amplitude is again initially selected to be $0{\cdot}75^\circ$ and the minimum and maximum frequencies are 0 and 40 Hz, with a sweep duration of $T = 2{\cdot}8$ s.

Typical theoretical results for the transverse r.m.s. deflection near the tip of the delta wing to a frequency sweep gust excitation are shown in Figure 7(a,b) for $U = 20$ m/s and $\alpha_0 = 1^\circ$. Figure 7(a) corresponds to an increasing frequency sweep, and 7(b) to a decreasing frequency sweep. From the envelope of this time response, no jump phenomenon is seen for either the increasing or the decreasing frequency gust, and the time corresponding to the maximum response amplitude is almost the same. For a linear frequency sweep gust, an instantaneous frequency is defined by

$$\omega = \frac{\mathrm{d}\phi}{\mathrm{d}t} = \omega_1 + \frac{\omega_2 - \omega_1}{T} t. \tag{6}$$

The present results for $\alpha_0 \neq 0$ are distinctly different from those for $\alpha_0 = 0$ that were discussed in Tang *et al.* (2000). For comparison, the results for $\alpha_0 = 0$ are shown in Figure 8(a) corresponding to an increasing linear frequency sweep gust excitation.

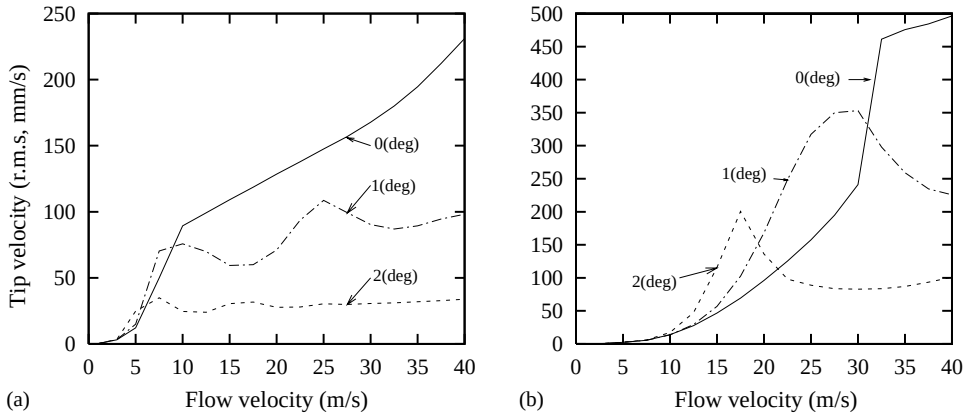

Figure 6. Tip r.m.s. velocity response versus the flow velocity: (a) $\omega_g = 10$ Hz; (b) $\omega_g = 20$ Hz.

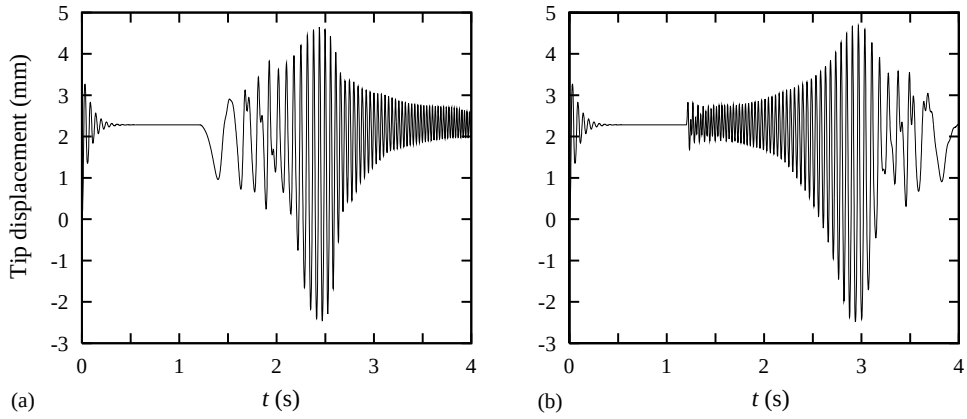

Figure 7. Gust response time history to a linear frequency sweep gust for $\alpha_0 = 1^\circ$ and $U = 20$ m/s: (a) an increasing linear frequency sweep; (b) a decreasing linear frequency sweep.

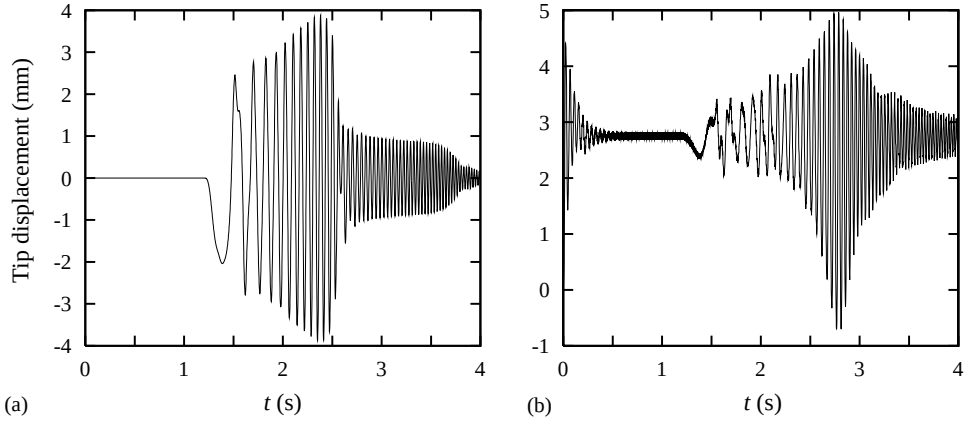

Figure 8. Gust response time history to a linear frequency sweep gust for $U = 20$ m/s: (a) $\alpha_0 = 0$; (b) $\alpha_0 = 2^\circ$. Increasing frequency sweep only is shown.

For $\alpha_0 = 0$, there is a clear jump phenomenon and the time corresponding to the maximum response amplitude is different for the increasing and decreasing frequency sweep. One is 2·25 s corresponding to an excitation frequency, $\omega = 15$ Hz; and the other is 3·19 s corresponding to $\omega = 11{\cdot}56$ Hz; [the latter is not shown here, see Tang *et al.* (2000)].

As is known from Figure 2, the delta wing model has a limit cycle oscillation when the flow velocity is in a certain range (without a lateral gust). Figure 8(b) shows the transverse response to a frequency sweep gust excitation for $U = 20$ m/s and $\alpha_0 = 2^\circ$. It is seen from this figure that there is an LCO with high frequency and small amplitude in the first 1·2 s of the time history. (Note that gust load is applied after 1·2 s.) The natural LCO response becomes very weak relative to the gust response after the gust excitation is applied. Indeed, it appears the gust excitation tends to suppress the LCO *per se*.

Figure 9 shows an FFT analysis of the response time history to a linear frequency sweep gust for $U = 20$ m/s and $\alpha_0 = 0$, 1 and 2°; recall Figures 7(a) and 8(a,b). We find the dominant peak frequency ("natural frequency" of the aeroelastic system) increases with increasing steady angle of attack from 15 Hz ($\alpha_0 = 0$) to 20·7 Hz ($\alpha_0 = 2^\circ$). Similarly to

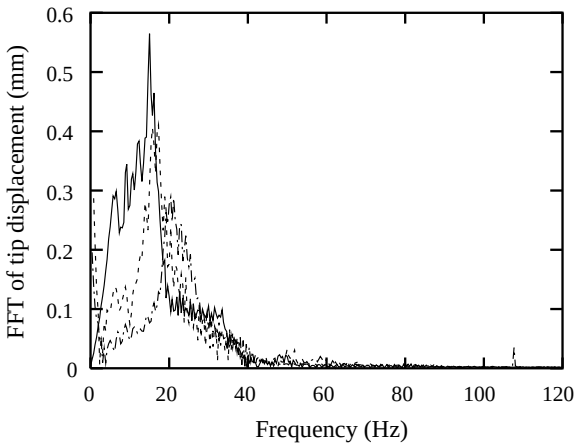

Figure 9. FFT analysis of the gust response for $U = 20$ m/s and $\alpha_0 = 0{,}1$ and 2° at the tip of wing: —, $\alpha_0 = 0^\circ$; - - -, $\alpha_0 = 1^\circ$; –·–, $\alpha_0 = 2^\circ$.

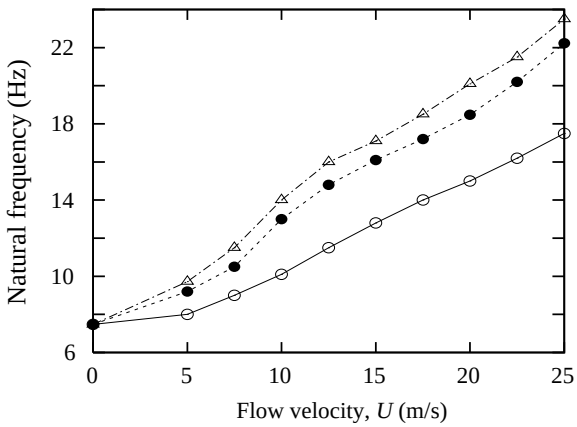

Figure 10. Dominant peak response frequency versus flow velocity: –○–, $\alpha_0 = 0^\circ$; - - -●- - -, $\alpha_0 = 1^\circ$; - - -Δ- - -, $\alpha_0 = 2^\circ$.

the results shown in Figure 9, for other flow velocities we can also determine a relationship between the dominant peak frequency and flow velocity for different steady angles of attack. The results are shown in Figure 10. The "natural frequency" of the aeroelastic system increases as the flow velocity and steady angle of attack increase.

4. CORRELATION BETWEEN THEORETICAL AND EXPERIMENTAL RESULTS

The experimental structural model has the same parameters as in the numerical example previously discussed. The clamped root of this model is fixed on a support mechanism which is placed at the top of the tunnel. The steady angle of attack can be adjusted. The delta wing model is mounted in a vertical position in the center of the test-section to eliminate gravitational preload in the out-of-plane direction. The first five *in vacuo* experimental natural frequencies are 7·5, 29·25, 35·25, 71·35 and 85·50 Hz, and the corresponding theoretical values are 7·47, 29·61, 33·84, 70·27 and 83·78. The agreement between the two results is good.

The gust was created by placing a rotating slotted cylinder (RSC) behind an airfoil upstream of the delta wing model. The gust generator configuration in the wind tunnel had two airfoils or vanes and two rotating slotted cylinders. The distance between these vanes was 12 in. For details of the gust generator design, see Tang *et al.* (1996). The gust conditions selected were those expected to give interesting linear and nonlinear response within the capacity of the experimental apparatus.

One of the reviewers has expressed concern about our ability to measure small gust angles. The measurement of gust angles in the 1–2° range of effective angle of attack has not proven to be a problem when using a calibrated pressure probe originally developed by the NASA Langley Research Center and adopted for our purposes here and in Tang *et al.* (1996). The principal uncertainty in modelling the experimental gust field as an input to our theoretical response calculations is the degree to which it may be treated as a single or multiple harmonic time-series. In our work, using a two harmonic approximation appears sufficient, with the most significant uncertainty being with respect to the assumption of zero phase shift between the first and second harmonics. Fortunately, the theoretical response results do not seem to be sensitive to the phase angle between the two harmonics.

Structural response measurements were made using the Ometron VPI 4000 Scanning Laser Vibrometer system (Ometron 1997). The VPI sensor is a noncontacting transducer that uses optical interferometry and electronic frequency measurements to determine the frequency shift of a beam of light reflected from a moving surface. The system then uses frequency-tracking methods to convert the frequency shift to an analog voltage corresponding to the velocity of the moving surface. Since there is no contact between the laser and the delta wing, the system is capable of making point velocity FFT or power spectrum measurements without altering the dynamics of the delta wing or the flow across it.

4.1. A Periodic Gust Excitation with Two Harmonics

Figure 11 shows the measured gust angle of attack, α_g, versus gust flow velocity for gust excitation frequencies, 8·5 and 15 Hz. See Tang *et al.* (1996) for details regarding the gust measurement. The solid and broken lines indicate a least-square curve fitting of the experimental data. The gust angle of attack varies with the gust frequency and is not a pure sinusoid. Hence, both the first (#1) and second (#2) harmonics of the gust are shown.

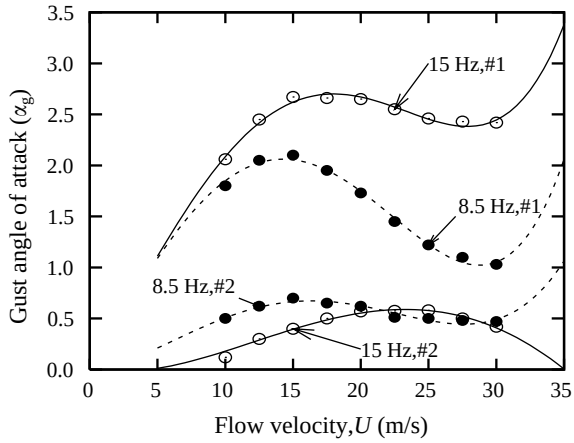

Figure 11. Gust angle of attack versus flow velocity for $\omega_g = 15$ and 8·5 Hz; first (#1) and second (#2) harmonics.

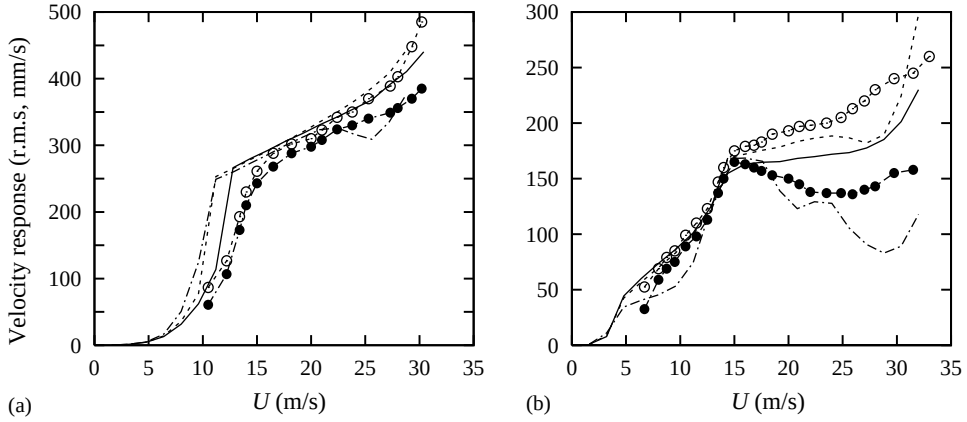

Figure 12. Tip velocity response (r.m.s.) versus flow velocity: (a) $\omega_g = 15$ Hz; (b) $\omega_g = 8{\cdot}5$ Hz. —, Theory, $\alpha_0 = 0^\circ$; - - - -, theory, $\alpha_0 = 1^\circ$; –●–, theory, $\alpha_0 = 2^\circ$; - -○- -, test, $\alpha_0 = 1^\circ$; - - -●- - -, test, $\alpha_0 = 2^\circ$.

The second harmonic component cannot be neglected. In the theoretical calculations for correlation with the measured response to a gust, we use the measured experimental gust angle of attack as the excitation including both the fundamental and second harmonic components of the gust angle of attack.

Figure 12(a) shows the correlation between the theoretical and experimental results for the tip velocity responses versus flow velocity and several steady angles of attack for a nominal gust excitation frequency of $\omega_g = 15$ Hz. For comparison, the theoretical results for $\alpha_0 = 0^\circ$ are also included in this figure as shown by a solid line. The experimental results for $\alpha_0 = 1$ and 2° are indicated by the symbols ○ and ●, respectively. The correlation between the theoretical and experimental results is reasonably good, especially for flow velocities higher than 15 m/s. Similar results for another gust excitation frequency, $\omega_g = 8{\cdot}5$ Hz, are shown in Figure 12(b). It is seen that the correlation between the theoretical and experimental results is also reasonably good. Note that the velocity response for $\alpha_0 = 2^\circ$ is smaller than that for $\alpha_0 = 1^\circ$ for both gust excitation frequencies.

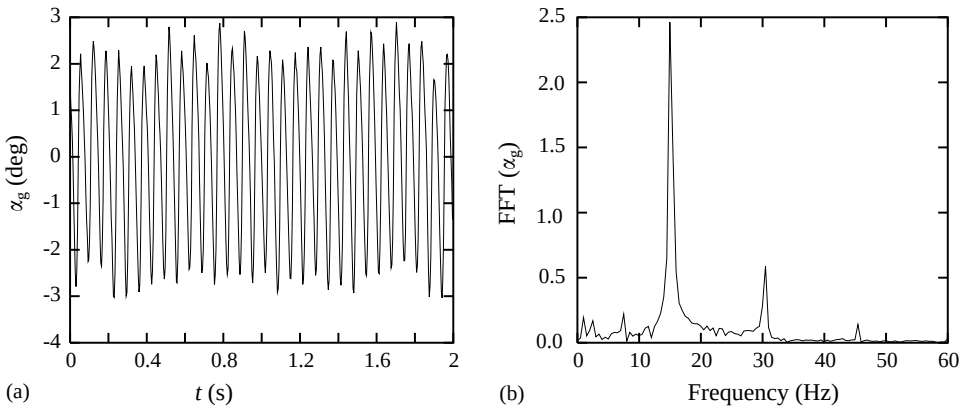

Figure 13. Experimental gust angle of attack for $U = 24{\cdot}5$ m/s and $\omega_g = 15$ Hz: (a) time history; (b) FFT analysis.

This is expected due to increasing (nonlinear) structural stiffness with increasing steady angle of attack.

Figure 13(a) shows the time history of the experimental gust angle of attack for $U = 24{\cdot}5$ m/s, $\omega_g = 15$ Hz and $\alpha_0 = 2^\circ$. Figure 13(b) shows the FFT of the time history of the gust angle of attack for the same condition. The dominant component of the gust angle of attack is $\alpha_{g1} = 2{\cdot}46^\circ$ and the corresponding gust velocity is $w_{g1} = U\alpha_{g1}$; the second harmonic component is $\alpha_{g2} = 0{\cdot}58^\circ$ or $w_{g2} = U\alpha_{g2}$. The theoretical gust velocity is constructed as follows:

$$w_g = w_{g1} \sin(2\pi\omega t - \Delta\phi) + w_{g2} \sin 2(2\pi\omega t - \Delta\phi).$$

Note that the phase difference between the first and second harmonic components of the gust velocity is neglected and this may be a source of the observed differences between theory and experiment. This effect appears to be small, however, based upon theoretical simulations with different phase angles.

Figure 14 shows the theoretical (a) and experimental (b) tip velocity time responses of the delta wing for $U = 24{\cdot}5$ m/s, $\omega_g = 15$ Hz and $\alpha_0 = 2^\circ$. Figure 15 shows the FFT of the theoretical and experimental time histories for the same condition. In this case, the correlation is good.

Next, the frequency response behavior of this aeroelastic system is discussed. Figure 16 shows a measured gust angle of attack (α_g) versus gust excitation frequency (Hz) for the flow velocity $U = 15$ m/s. The solid and broken lines indicate the least-square curve fitting of the experimental data for the first (#1) and second (#2) harmonics, respectively. Note the gust angle varies with the gust frequency and is not a pure sinusoid. In the following theoretical calculations, we again use the measured experimental gust angle of attack as the excitation for comparison with the experimental gust response results.

Figure 17 shows the correlation between the theoretical and experimental results for the tip velocity responses versus gust excitation frequency and several steady angles of attack at the flow velocity $U = 15$ m/s. For comparison, the theoretical results for $\alpha_0 = 0^\circ$ are also plotted in this figure as shown by the solid line. Both the theoretical and experimental results show the resonant frequency of the aerodynamic system increases as the steady angle of attack increases. The correlation for peak response amplitude is reasonably good;

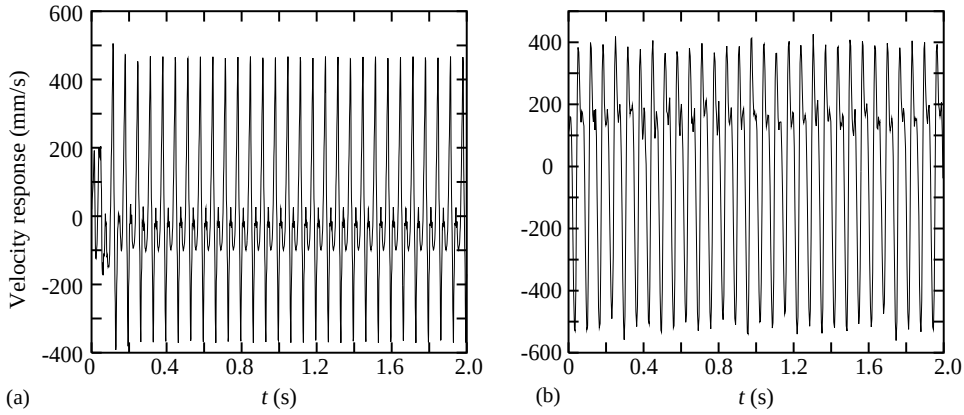

Figure 14. Tip velocity response behavior for $U = 24{\cdot}5$ m/s, $\alpha_0 = 2^\circ$ and $\omega_g = 15$ Hz: (a) theoretical time history; (b) experimental time history.

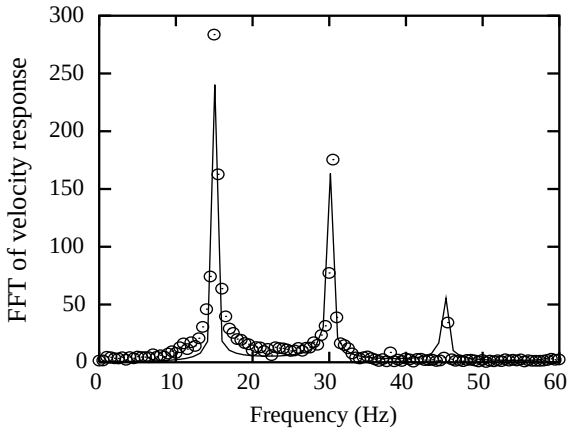

Figure 15. FFT analysis of gust velocity response behavior for $U = 24{\cdot}5$ m/s, $\alpha_0 = 2^\circ$ and $\omega_g = 15$ Hz: —, theory; ◦, test.

however, the correlation between the theoretical and experimental results is not as good for the resonant frequency.

It appears the theoretical model predicts a larger increase in structural stiffness due to static aerodynamic loading than is observed in the experiments.

4.2. A Frequency Sweep Gust Excitation

Figure 18(a) shows a measured continuous increasing linear frequency sweep gust angle of attack for $U = 25$ m/s. The minimum and maximum frequencies are 0 and 40 Hz, and the sweep duration T is 2·7 s. It is noted that the measured lateral gust has about a 0·3 s time delay corresponding to the restarting time of the DC-motor for each repeated sweep due to its rotational inertia. For convenient application, a theoretical gust excitation is constructed based upon the experimental gust data:

$$w_g(t) = \bar{w}_{gs}(t) \sin\left(\omega_1 + \frac{\omega_2 - \omega_1}{2T} t\right) t, \tag{7}$$

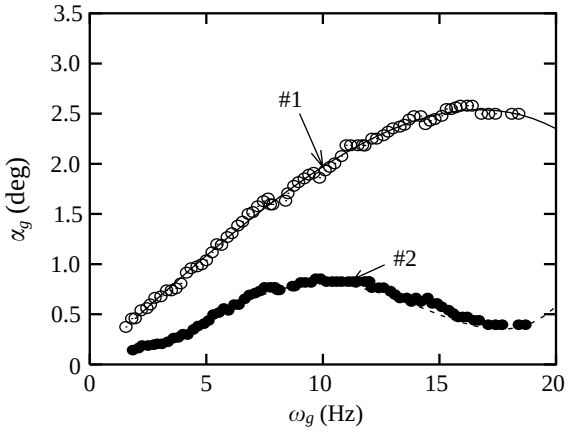

Figure 16. Gust angle of attack versus gust frequency for $U = 15$ m/s: first (#1) and second (#2) harmonics.

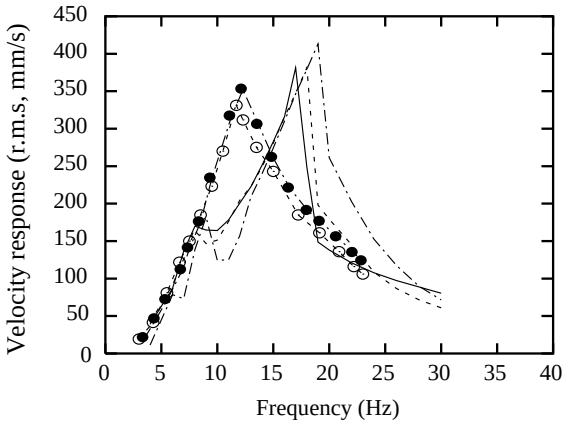

Figure 17. Velocity r.m.s. response versus frequency for $U = 15$ m/s. Theory: —, $\alpha_0 = 0°$- - - -; $\alpha_0 = 1°$; –●–, $\alpha_0 = 2°$. Experiment: - -○- -, $\alpha_0 = 1°$; - -●- -, $\alpha_0 = 2°$.

where $w_{gs}(t)$ is given by

$$w_{gs}(t) = \begin{cases} 0 & 0 < t < 0{\cdot}3 \text{ s}, \\ \sum_{i=0}^{4} c_i t^i & 0{\cdot}3 \text{ s} \leq t \leq 3{\cdot}0 \text{ s}. \end{cases} \tag{8}$$

The coefficients $c_0, \ldots, c_4$ are determined by a least-square curve fitting method from the experimental data. The fitted curve of the measured continuous linear frequency sweep gust that is used in the theoretical calculations is shown in Figure 18(b). The PSD comparison between the theory and experiment for the gust excitation is shown in Figure 18(c). To the degree that the theoretically simulated gust excitation is a less than completely faithful representation of the measured data, the corresponding gust response results are expected to be less satisfactory in terms of theory versus experiment.

The theoretical and experimental results for the tip velocity response are shown in Figures 19(a) and 19(b) for $\alpha_0 = 2°$ and flow velocity $U = 25$ m/s. Note that only one sweep period is shown. The corresponding FFT analysis is shown in Figure 20. There are ten sweep periods in 30 s and the total sampling length is 51, 200 points for the experimental data. In this figure, both theoretical (solid line) and experimental (dashed

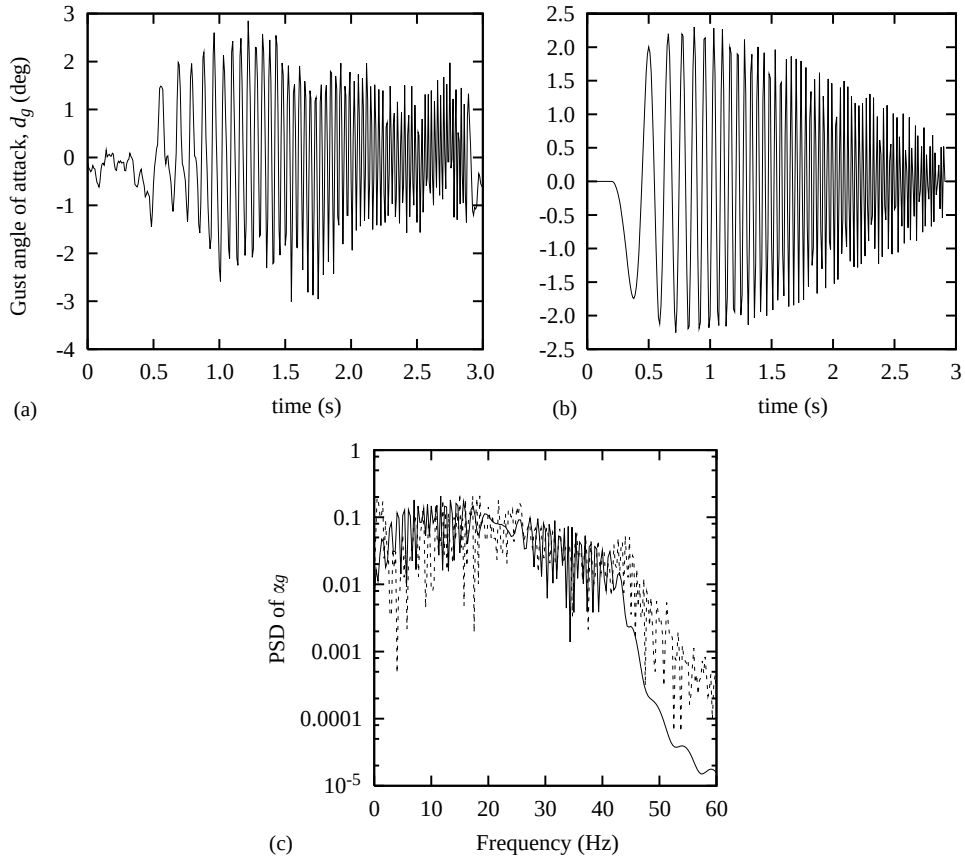

Figure 18. A continuous linear frequency sweep gust angle of attack for $U = 25$ m/s: (a) measured data; (b) numerical simulation. (c) PSD analysis of theoretical (—) and experimental (- - -) gust angle of attack.

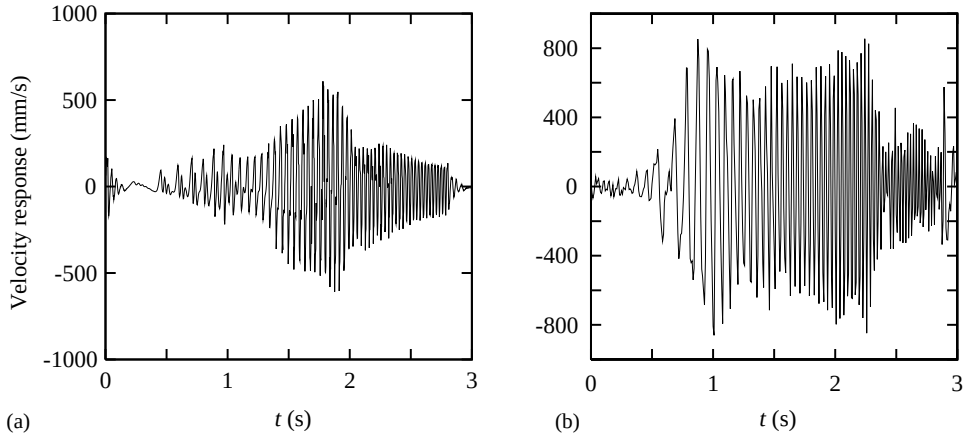

Figure 19. Velocity response to a continuous linear frequency sweep gust for $U = 25$ m/s and $\alpha_0 = 2°$: (a) theoretical data; (b) measured data.

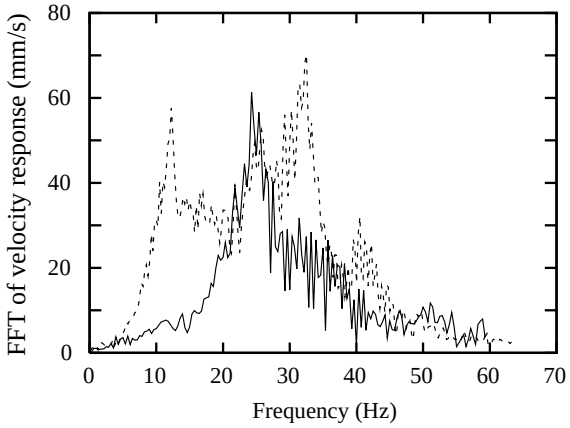

Figure 20. FFT analysis of theoretical and experimental velocity response to frequency sweep gust for $U = 25$ m/s and $\alpha_0 = 2^0$: —, theory; - - -, experiment.

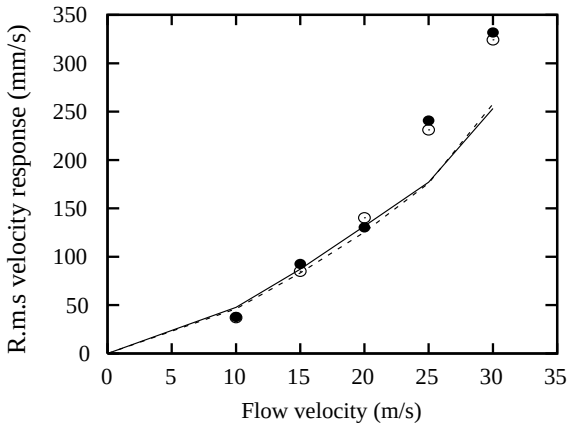

Figure 21. Theoretical and experimental r.m.s. velocity response to frequency sweep gust versus flow velocity for $\alpha_0 = 1$ and 2°. Theory: —, $\alpha_0 = 1°$; - - -, $\alpha_0 = 2°$; experiment: ●, $\alpha_0 = 1°$; ○, $\alpha_0 = 2°$.

line) results are shown for an average over ten sweep periods. It is very clear that the theoretical resonant frequency is 23·5 Hz for this aeroelastic system. However, significant experimental response occurs at several resonant frequencies of this aeroelastic system, i.e., at 12, 24, 32 and 40 Hz. Good theoretical–experimental correlation at 23·5 Hz is seen, but not at 12 and 32 Hz. These differences in gust response are likely due primarily to differences between the theoretical representation of the gust angle of attack and the actual experimental gust. Of course, measuring the gust itself is not without error [see Tang *et al.* (1996)].

Figure 21 shows the r.m.s. velocity response versus flow velocity and a comparison between the theoretical and experimental results for $\alpha_0 = 1$ and 2°. The r.m.s. amplitude is constructed from ten sweep periods in 30 s for the experimental data. The calculated and measured r.m.s. amplitudes are in good agreement at flow velocities lower than 20 m/s, but for higher flow velocities there is a larger difference. Both the theoretical and experimental r.m.s. amplitudes show a slight difference between those for $\alpha_0 = 1°$ and those for $\alpha_0 = 2°$. For the lower flow velocities, the agreement between theory and experiment is better for the FFT (not shown) as well as the r.m.s. response.

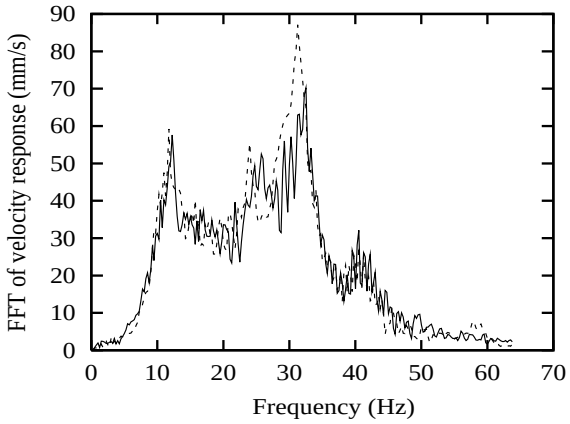

Figure 22. FFT analysis of experimental velocity response to frequency sweep gust for $U = 25$ m/s: - - -, $\alpha_0 = 1^\circ$; - - -, $\alpha_0 = 2^\circ$.

Figure 22 shows the FFT results and comparison between the experimental results of $\alpha_0 = 1$ and 2° for the flow velocity $U = 25$ m/s. The solid line indicates the results for $\alpha_0 = 2^\circ$ and the dashed line indicates the results for $\alpha_0 = 1^\circ$. As the steady angle of attack increases, the aeroelastic resonant frequencies also increase, but the response decreases slightly.

The agreement between theory and experiment for the r.m.s. response is better than that for the FFT, as expected. Indeed, the agreement for r.m.s. response is surprisingly good. Even the larger differences at higher flow velocities are relatively modest given the complexity of the dynamical system and its excitation.

5. CONCLUSIONS

The nonlinear structural response of a delta wing model to a periodic gust at different steady angles of attack has been studied. Results for a single and double harmonic gust as well as for a frequency sweep gust have been computed and measured. The fair to good quantitative agreement between theory and experiment verifies that the effects of steady angle of attack on the nonlinear aeroelastic response can be modelled and may significant. This is because the delta wing-plate stiffness increases as the steady angle of attack increases for a given flow velocity due to the plate nonlinearity.

ACKNOWLEDGEMENTS

This work was supported under AFOSR Grant, "Limit Cycle Oscillations and Nonlinear Aeroelastic Wing Response." Dr Daniel Segalman and Dean Mook are the grant program officers. All numerical calculations were done on a supercomputer, T916, in the North Carolina Supercomputing Center (NCSC).

REFERENCES

BUNTON, R. W. & DENEGRI JR, C. M. 2000 Limit cycle oscillation characteristics of fighter aircraft. *Journal of Aircraft* **37,** 916–918.

OMETRON 1997 VPI 4000 Scanning laser vibrometer operator's manual. Sterling, VA, U.S.A.
TANG, D. M. & DOWELL, E. H. 2001 Effects of angle of attack on nonlinear flutter of a delta wing. *AIAA Journal* **39,** 15–21.
TANG, D. M., CIZMAS, P. G. A. & DOWELL, E. H. 1996 Experiments and analysis for a gust generator in a wind tunnel. *Journal of Aircraft* **33,** 139–148.
TANG, D. M., HENRY, J. K. & DOWELL, E. H. 1999 Limit cycle oscillations of delta wing models in low subsonic flow. *AIAA Journal* **37,** 1355–1362.
TANG, D. M., HENRY, J. K. & DOWELL, E. H. 2000 Nonlinear aeroelastic response of a delta wing to periodic gust. *Journal of Aircraft* **37,** 155–164.

APPENDIX: NOMENCLATURE

A, B	vortex lattice aerodynamic coefficient matrices
c	delta wing root chord
D	delta wing-plate bending stiffness
E	Young's modulus
h	delta wing-plate thickness
km, kn	numbers of vortex elements on delta wing in x-,y-direction, respectively
kmm	total number of vortices on both the delta wing and wake in the x-direction
L	delta wing span
m	delta wing panel mass/area, $m = h\rho_m$
mxy	number of delta wing structural modal functions in the x-,y-plane defining u, v
nxy	number of delta wing structural modal functions in the z-direction defining w
q_n	generalized coordinate in the z-direction
R_a	size of reduced order aerodynamic model
t	time
U	airspeed
U_f	flutter airspeed
w	plate transverse deflection
w_g	gust velocity
W_k	transverse modal function in z-direction
x, y	streamwise and spanwise coordinates
X, Y	right and left eigenvector matrices of vortex lattice eigenvalue model
z	normal coordinate
Z	eigenvalue matrix of vortex lattice aerodynamic model
α_0	steady angle of attack
α_g	gust angle of attack
Γ	the vortex strength
Δt	the time step, $\Delta x/U$
Δx	plate element length in the streamwise direction
ρ_∞, ρ_m	air and plate densities
τ	time parameter, $\sqrt{mc^4/D}$ (s)
ω	frequency
ω_g	gust frequency
$(\dot{})$	$\mathrm{d}(\,)/\mathrm{d}t$